https://doi.org/10.5194/egusphere-2025-19
Preprint. Discussion started: 7 February 2025


# Assimilation of GNSS Zenith Delays and Tropospheric Gradients: A Sensitivity Study utilizing sparse and dense station networks

Rohith Thundathil[1,2], Florian Zus[2], Galina Dick[2], Jens Wickert[1,2]

[1]Technische Universität, Berlin, Germany
[2] German Research Centre for Geosciences, GFZ Potsdam, Germany

*Correspondence to*: Rohith Thundathil (r.thundathil@tu-berlin.de)

**Abstract.** The assimilation of Global Navigation Satellite System (GNSS) zenith total delays (ZTDs) into numerical weather models improves weather forecasts. In addition, the GNSS tropospheric gradient (TG) estimates provide valuable insight into the moisture distribution in the lower troposphere. In this study, we utilize a newly developed forward operator for TGs to investigate the sensitivity effects of incorporating TGs into the Weather Research and Forecasting model at varying station network densities. We assimilated ZTD and TGs from sparse and dense station networks (0.5 and 1-degree). Through this study, we found that the improvement in the humidity field with the assimilation of ZTD and TGs from the sparse station network (1-degree resolution) is comparable to the improvement achieved by assimilating ZTD only from the dense station network (0.5-degree resolution). These results encourage the assimilation of TGs alongside ZTDs in operational weather forecasting agencies, especially in regions with few GNSS stations. Conversely, assimilating TGs alongside ZTDs from sparse GNSS networks can be a cost-effective way to enhance the accuracy of the model fields and subsequent forecast quality.

## 1 Introduction

Global Navigation Satellite Systems (GNSS) have become integral to our everyday lives. It significantly revolutionized how we determine our position, navigate, and keep track of time. The most profound application of GNSS has been in civilian and commercial uses, such as positioning, navigation, and timing. However, GNSS is increasingly valuable for geosciences in accurately sensing atmospheric and surface properties and other geophysical parameters. Additionally, it can be used to derive the Earth's surface properties, deformation, and other geophysical parameters (Wickert et al., 2020).

Monitoring atmospheric water vapor with GNSS regional ground networks has helped bridge gaps in established meteorological observing systems. GNSS is distinguished from other observation systems by its numerous benefits, such as low operating costs, all-weather availability, and exceptional spatio-temporal resolution. The total number of GNSS stations worldwide exceeds 10,000. European networks, with about 3,000 stations, enhance regional weather forecasts. Incorporating advanced GNSS-based observations allows us to provide high-quality information with high spatio-temporal distribution in

https://doi.org/10.5194/egusphere-2025-19
Preprint. Discussion started: 7 February 2025


operational weather forecasting models worldwide. This is essential for accurately modeling the atmosphere, especially for predicting heavy precipitation and severe weather events, which are significant challenges in weather research.

Since 1992, GNSS signals have been utilized to monitor the atmosphere through ground-based stations ('GNSS meteorology'). GNSS meteorology uses the time delay of radio signals traveling from the satellite to the station to monitor atmospheric water vapor. Zenith Total Delay (ZTD) is a key measurement in GNSS meteorology (Bevis et al., 1992), closely linked to the Integrated Water Vapor (IWV) above the station. ZTD data are available in near-real-time (NRT) from several European station networks, such as the European Meteorological Network Global Navigation Satellite Systems Water Vapor Program (EGVAP). Once adjusted for ionospheric effects, the delay caused by the troposphere in transmitting GNSS signals between satellites and stations is estimated. The ZTD has been utilized by various operational forecast agencies. Several assimilation studies have been performed with ZTDs and found that they enhance the accuracy of the forecasts. For example, Vedel and Huang (2004) showed that the ZTD assimilation improved the prediction of strong precipitation. Poli et al. (2007) also found a positive impact on the prediction of short-term precipitation and quantitative precipitation forecast scores for total precipitation over France between +12 and +36 hours after analysis time. The Action de Recherche Petite Échelle Grande Échelle (ARPEGE) global model was used here to understand the assimilation impact of synoptic-scale circulations and precipitation forecasting during spring and summer. Yan et al. (2009) performed assimilation experiments using the Aire Limitée Adaptation Dynamique Développement International (ALADIN) model. They found that assimilating ZTDs improved the meso-nonhydrostatic precipitation forecasts for a heavy rainfall event over the Mediterranean region. Boniface et al. (2009) assimilated GNSS data into the Applications of Research to Operations at Mesoscale (AROME) model. They showed improvement in predicting the spatial extent of the precipitation. Lindskog et al. (2017) used the HIRLAM–ALADIN (High Resolution Limited Area Model; Aire Limitée Adaptation Dynamique Développement International) Research on Mesoscale Operational NWP in Euromed (HARMONIE) Applications of Research to Operations at Mesoscale (HARMONIE–AROME) model to test ZTD data assimilation. Their findings show that including ZTD as an additional observation type enhances forecast accuracy, emphasizing the possibility of enhancing data assimilation by combining GNSS ZTD with other observations. Rohm et al. (2019) conducted assimilation studies using the Weather Research and Forecast (WRF) model ZTD operator. They found that the ZTD assimilation altered the moisture field and precipitation rather than other parameters, such as the pressure or temperature field. GNSS observations enhance forecasts within 24 hours, with the most impact at a 9-hour lead time. Giannaros et al. (2020) and Caldas-Alvarez and Khodayar (2020) also demonstrated the significant benefits of incorporating GNSS ZTD data to improve precipitation and water vapor forecasts. Their studies used the WRF model in a broader Mediterranean region and the COSMO-CLM (COnsortium for Small-scale MOdeling in CLimate Mode) model in the central European region, respectively. Lagasio et al. (2019) discovered that integrating diverse Sentinel-1 and GNSS ZTD observations into the WRF model provides significant advantages for forecasts, offering detailed information on the wind field and water vapor content. Singh et al. (2019) found that using ZTD observations from a ground-based GNSS network improved humidity, air temperature, and wind forecasts in the Indian region. Assimilating these observations reduced forecast errors in wind fields and enhanced rainfall predictions to some

https://doi.org/10.5194/egusphere-2025-19
Preprint. Discussion started: 7 February 2025


extent. Mascitelli et al. (2019, 2021) successfully utilized the Regional Atmospheric Modeling System at the Institute of Atmospheric Sciences and Climate (RAMS@ISAC) model to incorporate GNSS ZTD data, leading to a significant enhancement in short-term water vapor prediction with minimal impact on precipitation forecasts. Yang et al. (2020) found that combining ZTD and radar data improved the accuracy of heavy rainfall location and intensity. They also discovered that using a broader horizontal localization scale instead of the convective scale for radar data assimilation enhanced the impact of ZTD data. Risanto et al. (2021) found that assimilating Global Positioning System (GPS) precipitable water vapor improved short-range North American monsoon precipitation forecasts by reducing errors and biases in the initial conditions of the weather model. This enhanced the model's ability to capture nocturnal convection of mesoscale convective systems and improved precipitation timing.

ZTDs are the only source of moisture data used operationally; however, they provide limited atmospheric information. New observations must augment the existing observations, providing additional information. According to Bennitt & Jupp (2012) and Mahfouf et al. (2015), the limitations of ZTD lie in its inability to provide information on horizontal or vertical atmospheric gradients. Tropospheric gradient (TG) is another variable derived from the GNSS (Bar-Sever et al., 1998). In simple terms, TGs mainly provide information on the moisture's change (or "gradient") in a specific direction. Bar-Sever et al. (1998) showed that including TGs in GPS geodesy enhances accuracy and precision, with the estimated gradients matching real atmospheric moisture patterns observed by a water vapor radiometer (WVR). Walpersdorf et al. (2001) used the ALADIN model to validate GPS TGs at five stations. Iwabuchi et al. (2003) found a strong correlation between these gradients and moisture fields, with TGs typically pointing from dry to moist regions. Brenot et al. (2013) observed similar phenomena in their deep convection studies. Li et al. (2015) showed that better observation geometry improves gradient estimation accuracy. Morel et al. (2015) analyzed data from 12 Corsican stations using different software. Douša et al. (2016) analyzed data from hundreds of stations in central Europe and confirmed that GNSS TGs reflect real tropospheric features. Kačmařík et al. (2019) highlighted the sensitivity of TGs to processing options, emphasizing that real-time accuracy depends on high-quality satellite data.

Thundathil et al. (2024) illustrate the operator implementation and assimilation of TGs in the WRF model. The TG operator (Zus et al., 2023) was incorporated into the WRF data assimilation (WRFDA) system in version 4.4.1. The source codes are published online for the research community worldwide. The study accomplished a two-month assimilation impact study to obtain statistical confidence on the impact focused on Europe. The observations for the impact studies were collected from the Nevada Geodetic Laboratory (NGL). The study quantified the impact, showing promising improvements by adding TGs on top of ZTDs. In this study, we aim further to investigate the potential of TGs through a sensitivity experiment. We wish to analyze under which circumstances TGs provide information when combined with ZTDs to improve the initial conditions for numerical weather prediction.

https://doi.org/10.5194/egusphere-2025-19
Preprint. Discussion started: 7 February 2025


## 2. GNSS ZTD and Tropospheric Gradients

The tropospheric delay is caused by the signal traveling through the neutral atmosphere. It is parameterized in the GNSS analysis with mapping functions (MFs), zenith delay, and gradient terms. The tropospheric delay $T$ at the station is expressed as a function of the elevation angle $e$ and the azimuth angle $a$:

$$T(e,a) = m_h(e).Z_h + m_w(e).Z_w + m_g(e)[\cos(a).N + \sin(a).E] \quad (1)$$

where $Z_h$ is the zenith hydrostatic delay (ZHD), $Z_w$ is the zenith wet delay (ZWD), and $N$ and $E$ are the north and east gradient components. The hydrostatic, wet, and gradient MFs are denoted $m_h$, $m_w$, and $m_g$, respectively. The ZTD, $Z$, is given by

$$Z = Z_h + Z_w. \quad (2)$$

The forward operator for the ZTD, along with the tangent linear and adjoint operators, is already integrated into the WRFDA system. The ZTD is calculated through:

$$Z = 10^{-6} \int \Psi \, dz \quad (3)$$

where the refractivity, $\Psi$, is a function of pressure, temperature, and humidity (Thayer, 1974), with $z$ denoting the height above the station. In the GNSS data analysis, the ZTD $(Z)$, the north gradient component $(N)$, and the east gradient component $(E)$ are estimated with geodetic parameters through least square adjustment (Gendt et al., 2004). The three quantities, depending on the state of the atmosphere in the vicinity of the station, are considered observations. The TG forward operator uses a fast approach which works as follows: for the given station location, we utilize a closed-form expression that depends on the north–south and east–west horizontal gradients of refractivity (as outlined in Davis et al., 1993). This enables the calculation of the north and east gradient components through

$$N = 10^{-6} \int z\Psi_y dz \quad (4)$$

$$E = 10^{-6} \int z\Psi_x dz \quad (5)$$

Here, $x$, $y$, and $z$ represent the Cartesian coordinates and partial derivatives are denoted by the corresponding subscripts. Similar to the computation of ZTDs, the TGs are also calculated using numerical integration.

Recently, Zus et al. (2023), developed the TG operator, which has been implemented into the WRFDA system version 4.4.1. Initial DA experiments conducted for the dense GNSS station network in Germany have shown promising results (Thundathil et al., 2024).

https://doi.org/10.5194/egusphere-2025-19
Preprint. Discussion started: 7 February 2025


## 3. Model setup

In this study, the WRF model version 4.4.1 is used with the Advanced Research WRF (ARW) core (Skamarock et al., 2008). WRF has been widely used for research within a large community and also serves as a model for operational forecasting at various agencies worldwide (Powers et al., 2017).

The model domain was configured with a 0.1-degree (approx. 11 km) horizontal resolution and 250 x 250 grid points. The number of vertical levels in the model is 50, extending from Earth's surface to an altitude of 50 hPa. The initial and boundary conditions were obtained from the European Centre for Medium-Range Weather Forecasts operational analysis, which had a spatial resolution of 0.14 degrees (approx. 16 km). Figure 1 shows the model domain with the GNSS stations.

The WRF model physics settings are the same as those in Thundathil et al. (2024). The radiation parameterization scheme used in this study is based on the Rapid Radiative Transfer Model for General Circulation Models (RRTMG) developed by Iacono et al. (2008). This model is recognized for its accuracy and efficiency in calculating long-wave and short-wave fluxes and heating rates, making it particularly suitable for applications in general circulation models.

For the cloud microphysics, we implemented the Thompson double-moment scheme (Thompson et al., 2008), which can predict mixing ratios for cloud water, rain, ice, snow, and graupel. The planetary boundary layer scheme utilized in this simulation is the Yonsei University (YSU) scheme (Hong et al., 2010; Hong & Lim, 2006). The YSU is a non-local scheme with first-order closure that incorporates counter-gradient and explicit entrainment terms into the turbulence flux equation.

This study also employed the unified Noah land surface model (Chen & Dudhia, 2001). This model consists of four layers and is designed to predict soil temperature and moisture, canopy moisture, and snow cover. It takes into account various factors, including root zone dynamics, evapotranspiration, soil drainage, runoff, vegetation categories, and soil texture. This comprehensive approach yields valuable information on sensible and latent heat fluxes related to the boundary layer, including an enhanced treatment for urban areas.

To simulate the model accurately at a non-convective-scale resolution, it is crucial to include convection parameterization, which helps represent the statistical effects of sub-grid-scale convective clouds. For this purpose, we used the Grell–Freitas ensemble scheme (Grell & Freitas, 2014), which integrates a probability density function with data assimilation techniques.

### 3.1 DA Framework

In this study, we used the deterministic three-dimensional variational (3DVAR) DA system. It uses an iterative minimization of the cost function $J$ with a background constraint and an observation constraint. The 3DVAR cost function equation is given by

$$J(x) = \frac{1}{2}(x - x_b)^T \mathbf{B}^{-1}(x - x_b) + \frac{1}{2}(y - \mathbf{H}(x))^T \mathbf{R}^{-1}(y - \mathbf{H}(x)) \tag{6}$$

The variables $x$, $x_b$, and $y$ are column vectors that represent the model state, the background (or first guess), and the observation state, respectively. The forward operator, denoted by $\mathbf{H}$, maps the model state vector to the observation vector. $\mathbf{B}$ represents the background error covariance matrix, while $\mathbf{R}$ represents the observation error covariance matrix. The observations are assumed to be uncorrelated, so **R** is a diagonal matrix. **B** is a square, positive, semi-definite, and symmetric matrix that contains the variances of the background forecast errors along the diagonal and their covariances in the upper and lower triangles of the matrix. We computed a climatological background error covariance matrix using the National Meteorological Center (NMC) method (Parrish & Derber, 1992). The NMC method involves calculating forecast difference statistics to obtain the forecast error covariance. For regional simulations, forecast statistics are calculated by analyzing forecast differences over a month, using both 24-hour and 12-hour predictions. The statistics were derived from May 2013. We selected the 'CV5' option in the WRFDA system.

The assimilation system used a rapid update cycle (RUC) framework, with six-hourly assimilations over May and June 2013. We conducted two sets of experiments. The first set comprised three experiments: 1) Control run with assimilation of conventional data only, 2) ZTD run assimilating ZTDs on top of the Control run, and 3) ZTDGRA run assimilating ZTDs and TGs on top of the Control run. We term the second and third experiments ZTD_0.5° and ZTDGRA_0.5° to distinguish them from the second set of experiments, making them easier for readers to understand. In the RUC, an hourly forecast output was generated after each assimilation cycle for the next five hours, which resulted in one analysis and five forecasts. The second set of experiments was performed to analyze the sensitivity of the gradient observations by de-densification of the GNSS stations. We de-densified the GNSS stations from a roughly 0.5-degree to a 1-degree station network and then performed the assimilation experiments. Hence, ZTD_1.0° and ZTDGRA_1.0° runs were conducted similarly to ZTD_0.5° and ZTDGRA_0.5°, respectively, but with the assimilation of observations from the 1-degree station network. The assimilation cycle starts from 5 May 2013 00 UTC to 29 June 2013 18 UTC, the entire available data timeline from the benchmark campaign. The DA framework of the experiments is shown in Figure 2.

### 3.2 Data

For the assimilation experiment, we had GNSS tropospheric products from 430 stations which belong to the core of the Benchmark data set which was collected within the European COST Action ES1206 GNSS4SWEC (Advanced GNSS tropospheric products for monitoring severe weather and climate; Douša, Jan, et al., 2016). The GNSS ZTDs and TGs were obtained in precise point positioning mode utilizing the G-Nut/Tefnut software (Václavovic et al., 2014). Details on the quality of the tropospheric products can be found in Kačmařík et al. (2019). To ensure a homogeneous set of observations across the domain, we excluded collocated and clustered stations and specifically chose GNSS stations with data availability exceeding 75%. In addition, to comply with our WRF model domain, we carried out a simple thinning of observations. We obtained a station network with a resolution of about 0.5 degrees. After these steps, we were left with around 250 GNSS stations over the Benchmark domain. For the sensitivity experiment, we created another thinned station network with a resolution of about 1 degree that contained around 110 stations (see Fig. 1). In order to compare the simulations with respect to independent GNSS observations, we removed around 18 stations in Germany from the total dataset. The two months of simulation from the control experiment were employed to perform a station-specific bias correction for the GNSS ZTDs and TGs. Following the approach of Thundathil et al. (2024), we assigned an observation error of 8 mm for the ZTD and

https://doi.org/10.5194/egusphere-2025-19
Preprint. Discussion started: 7 February 2025


0.65 mm for the gradient for all observations. To improve the capabilities of the DA system, we set up a thorough network of surface reports across Europe. Radiosonde measurements offered a detailed view of the atmospheric thermodynamic structure at launch points. To address the underrepresentation of the radiosonde network during specific periods, such as 06:00 and 18:00 UTC rather than 00:00 and 12:00 UTC, we used a series of Tropospheric Airborne Meteorological Data Reporting (TAMDAR) observations.

## 4. Results

### 4.1 Impact of GNSS data

To evaluate the impact of assimilating TGs on top of ZTDs, we conducted a comparative analysis of the results from two-month-long assimilation experiments using data from GNSS stations. Specifically, we compared the analyses and forecasts obtained from these experiments against observations from GNSS stations, both assimilated and independent stations (which were not assimilated). The quantitative comparison involved hourly GNSS station data, which were assessed against six-hourly data assimilation (DA) analyses and five-hour forecasts initialized from these analyses. This section focuses on comparing the first set of experiments, labeled ZTD_0.5° and ZTDGRA_0.5°, with the control run.

Figure 3 summarizing station-specific root mean square error (RMSE) values (station specific RMSE plots are provided in the appendices) clearly demonstrate that the ZTDGRA_0.5° experiment yielded the lowest mean RMSE values for the ZTD parameter among all runs. This indicates the successful impact of gradient assimilation. Specifically, the mean RMSE for the ZTD variable decreased from 14.4 mm in the control run to 8.3 mm in the ZTD_0.5° run, and further to 8.2 mm in the ZTDGRA_0.5° run. Improvements were observed not only in ZTD values but also in the gradient components. Both the north and east gradient components exhibited reductions in RMSE. For the north gradient, RMSE decreased from 0.62 mm in the control run to 0.52 mm in the ZTD_0.5° run, and further to 0.49 mm in the ZTDGRA_0.5° run. Similarly, for the east gradient, RMSE decreased from 0.66 mm in the control run to 0.54 mm in the ZTD_0.5° run, and then to 0.50 mm in the ZTDGRA_0.5° run. These reductions in RMSE values underscore the significant improvements achieved by assimilating TGs, which enhanced the moisture field representation in the model state. The findings highlight the synergistic relationship between ZTDs and TGs assimilation, where assimilating ZTDs contributes to the refinement of TG components, and vice versa.

To confirm that these improvements were not solely due to comparisons with observations from the assimilated GNSS stations, we extended the analysis to include 18 independent GNSS stations that were excluded from the assimilation process. The RMSE for the ZTD variable decreased from 13.7 mm in the control run to 8.2 mm in the ZTD_0.5° run, and further to 8.0 mm in the ZTDGRA_0.5° run. Similar trends were observed for the gradient components. For the north gradient, RMSE decreased from 0.59 mm in the control run to 0.49 mm in the ZTD_0.5° run and 0.47 mm in the ZTDGRA_0.5° run. For the east gradient, RMSE reduced from 0.63 mm in the control run to 0.51 mm in the ZTD_0.5° run, and then to 0.48 mm in the ZTDGRA_0.5° run.

https://doi.org/10.5194/egusphere-2025-19
Preprint. Discussion started: 7 February 2025


These consistent results across both assimilated and independent GNSS station data demonstrate the robust improvements achieved through gradient assimilation on top of ZTDs. The two-month-long statistical evaluation confirms that the combined assimilation of ZTDs and TGs significantly enhances the accuracy of the model's analyses and forecasts, particularly in representing the humidity field.

### 4.2 Sensitivity analysis

A sensitivity experiment was conducted to better understand the conditions under which the assimilation of TGs, in addition to ZTDs, improves the representation of the humidity field. For this purpose, a second set of experiments was designed using GNSS data assimilation from a sparser 1-degree network. This allowed for a focused analysis of the additional impact brought by gradient assimilation. As with the dense network experiments, two configurations were tested: a ZTD assimilation run (ZTD_1.0°) and a combined assimilation run incorporating both ZTDs and TGs (ZTDGRA_1.0°).

When comparing data from stations included in the assimilation process, the ZTDGRA_1.0° experiment exhibited the lowest mean RMSE values for ZTD, similar to the results observed with the dense network configuration. Specifically, the ZTD variable's mean RMSE decreased from 14.4 mm in the control run to 9.2 mm in the ZTD_1.0° run and further to 8.7 mm in the ZTDGRA_1.0° run. For the TGs, RMSE values showed improvements in both the north and east components. The north gradient RMSE reduced from 0.63 mm in the control run to 0.55 mm in the ZTD_1.0° run and to 0.51 mm in the ZTDGRA_1.0° run. Similarly, the east gradient RMSE decreased from 0.66 mm in the control run to 0.58 mm in the ZTD_1.0° run and further to 0.52 mm in the ZTDGRA_1.0° run.

A comparable trend was observed with data from 18 independent GNSS stations excluded from the assimilation. For these stations, the ZTD variable's mean RMSE decreased from 13.7 mm in the control run to 9.0 mm in the ZTD_1.0° run and further to 8.5 mm in the ZTDGRA_1.0° run. The north gradient RMSE dropped from 0.59 mm in the control run to 0.52 mm in the ZTD_1.0° run and to 0.49 mm in the ZTDGRA_1.0° run. Similarly, the east gradient RMSE declined from 0.63 mm in the control run to 0.55 mm in the ZTD_1.0° run and further to 0.51 mm in the ZTDGRA_1.0° run.

From the RMSE values, we conclude that, in particular, for a sparse network configuration, we can expect a significant impact on the assimilation of TGs on top of ZTDs. For example, suppose we utilize the RMSE of ZTDs for the independent stations as an indication of the improvement in the (integrated) water vapor field. In that case, the drop in the RMSE from 8.2 mm in the ZTD_0.5° experiment to 8.0 mm in the ZTDGRA_0.5° experiment is smaller than the drop from 9.0 mm in the ZTD_1.0° experiment to 8.5 mm in the ZTDGRA_1.0° experiment. A similar trend can be seen when we utilize the RMSE of ZTDs for the 'allowed' stations.

The most striking feature was that the RMSE reduction of the ZTDGRA_1.0° run was similar to the ZTD_0.5° run. In other words, the assimilation of ZTDs and TGs from a sparse station network performed equally well as that of only ZTDs from the dense station network. In order to illustrate this visually, the analysis increments of ZTDGRA_1.0° and ZTD_0.5° runs for consecutive DA cycles were analyzed. Figure 4 shows five analysis increments from the first DA cycle on 6 May 2013 00 UTC until 7 May 2013 00 UTC, with assimilation every six hours. The rows in the plot refer to the corresponding DA

https://doi.org/10.5194/egusphere-2025-19
Preprint. Discussion started: 7 February 2025


cycles with ZTDGRA_1.0° on the left column and ZTD_0.5° on the right. The water vapor mixing ratio over the domain is vertically averaged for the first 16 model levels to portray the impact from the surface level up to the lower troposphere (approx. 6 km height). From the analysis increment comparison, a close match was observed between the two experiments with respect to respective assimilation cycles. From a visual inspection of the plots, the sparse-network assimilation of ZTD and gradient run had the same structures as seen in the dense-network assimilation of the ZTD alone run. Quantitatively, the similarity of the ZTD_0.5° and ZTDGRA_1.0° runs at respective assimilation cycles can be computed by the structural similarity (SSIM) index parameter. Hence, we computed the SSIM at all five assimilation cycles, showing a considerable similarity of the SSIM index greater than 0.98.

Finally, we took a closer look at the background and analyzed humidity profiles. We compared them with humidity profiles from the atmospheric reanalysis ERA5 (Hersbach et al., 2020) at five selected locations covering the area of interest. The RMSE of the profiles with respect to ERA5 averaged over the two months is shown in Figure 5. There were 220 DA cycles, and with five profile RMSE comparisons at each cycle, the total number of profiles totaled 1100. From the figure, the RMSE of the ZTDGRA_1.0° run appears to overlap with the ZTD_0.5° run. This shows that the information passed into the model when TGs are assimilated on top of ZTDs for sparse network configurations is roughly as effective as the assimilation of ZTDs from the dense network configuration. This finding is particularly relevant for those aiming to densify their existing GNSS networks for weather prediction purposes. Before the costly installation and maintenance of additional (single or dual frequency) GNSS stations, she/he should consider the assimilation of TGs on top of the ZTDs.

## 5. Conclusions

The TGs contain valuable information that has yet to be fully utilized by numerical weather models. From the assimilation experiments, we conclude that TGs, when assimilated in addition to ZTDs, enhance the accuracy of the humidity fields, thereby increasing the forecast accuracy. The work by Thundathil et al. (2024) already provided evidence that gradient observations positively impacted the analyses and forecast. The important result of this paper is the dependency of the impact of gradient observations on the network configuration. Since TGs can be roughly related to horizontal ZTD gradients, it was hypothesized that the impact of this new observation type would be beneficial, particularly for a sparse network configuration (Zus et al., 2019). Our results utilizing the state-of-the-art data assimilation system of WRF and GNSS tropospheric products from the Benchmark campaign prove this to be the case.

GNSS stations are available worldwide, but the station density varies from place to place. For example, the dense GNSS station network in Europe, with its near-real-time data provision capability, is already in its current status very effective in filling gaps in the humidity fields required for operational weather forecasting. However, in regions with a sparse GNSS station network or remote regions with isolated GNSS stations, the provided ZTD data leaves significant gaps in the highly variable humidity field. These gaps can be filled utilizing TGs.

https://doi.org/10.5194/egusphere-2025-19
Preprint. Discussion started: 7 February 2025


NWMs will run globally at high resolution in the near future. For instance, ECMWF's global operational forecast already has a resolution of 9 km. In the future, we will also have convection-permitting scale resolution models running on a global scale, which would demand more observations for their initialization. We expect that the assimilation of GNSS TGs, in addition to ZTDs, helps to close gaps in the knowledge of the humidity field.

## Appendices

A detailed analysis of the assimilation impact of the GNSS data products is depicted through additional figures. The six figures and the table in this section provide supporting information on how Figure 3 in the main article was derived. The specific impact of the assimilation due to ZTDs and TGs with both dense and sparse assimilation setups are shown through the standard deviation compared to each GNSS station. The statistics were derived using the analysis and compared to the assimilated GNSS stations and independent GNSS stations, which were excluded from the assimilation dataset. We term the assimilated stations “Allowed” and the independent stations “Excluded.” Please refer the Figures A1-A6. Additionally, the Table A1 will summarize all the mean values of the standard deviation for all the experiments to give a general overview of the impact of assimilation.

## Code and data availability statement

The model simulation data and the WRFDA code version 4.4.1, with the gradient operator codes, is available for download. It is stored on Zenodo, a general-purpose open repository developed under the European Open-Access Infrastructure for Research in Europe (OpenAIRE) program and operated by the European Organization for Nuclear Research (CERN). The access link is https://zenodo.org/doi/10.5281/zenodo.13734634.

## Author contributions

The original draft of the study was written by RT, who also conducted the formal analysis and experiments. FZ and RT collaborated to modify the WRFDA code and develop the gradient operator. JW and GD supervised the project, acquired funding, and reviewed and edited the paper.

## Competing interests

The contact author has declared that none of the authors has any competing interests.

## Acknowledgements

The research project is funded by the German Research Foundation (DFG; grant no. 68510200) and is titled "Exploitation of GNSS tropospheric gradients for severe weather Monitoring And Prediction (EGMAP)." The ECMWF conventional datasets for the DA study in this research were provided by Thomas Schwitalla from our collaborative institution, the Institute of Physics and Meteorology, University of Hohenheim, Stuttgart. The GNSS data are provided by the Geodetic Observatory Pecny (GOP) (http://www.pecny.cz (accessed on 25 February 2023)). We thank Michal Kačmařík for preparing the GNSS data set in a user-friendly format.

## References

Bar-Sever, Y. E., Kroger, P. M., & Borjesson, J. A. (1998). Estimating horizontal gradients of tropospheric path delay with a single GPS receiver. Journal of Geophysical Research: Solid Earth, 103(B3), 5019-5035. doi:10.1029/97JB03534

Bennitt, G. V., & Jupp, A. (2012). Operational assimilation of GPS zenith total delay observations into the Met Office numerical weather prediction models. Monthly Weather Review, 140(8), 2706-2719. doi:10.1175/MWR-D-11-00156.1

Bevis, M., Businger, S., Herring, T. A., Rocken, C., Anthes, R. A., & Ware, R. H. (1992). GPS meteorology: Remote sensing of atmospheric water vapor using the global positioning system. Journal of Geophysical Research: Atmospheres, 97(D14), 15787-15801. doi:10.1029/92JD01517

Boniface, K., Ducrocq, V., Jaubert, G., Yan, X., Brousseau, P., Masson, F., ... & Doerflinger, E. (2009, July). Impact of high-resolution data assimilation of GPS zenith delay on Mediterranean heavy rainfall forecasting. In Annales Geophysicae (Vol. 27, No. 7, pp. 2739-2753). Göttingen, Germany: Copernicus Publications. doi:10.5194/angeo-27-2739-2009

Brenot, H., Neméghaire, J., Delobbe, L., Clerbaux, N., De Meutter, P., Deckmyn, A., ... & Van Roozendael, M. (2013). Preliminary signs of the initiation of deep convection by GNSS. Atmospheric Chemistry and Physics, 13(11), 5425-5449. doi:10.5194/acp-13-5425-2013

Caldas-Alvarez, A., & Khodayar, S. (2020). Assessing atmospheric moisture effects on heavy precipitation during HyMeX IOP16 using GPS nudging and dynamical downscaling. Natural Hazards and Earth System Sciences, 20(10), 2753-2776. doi:10.5194/nhess-20-2753-2020

Douša, J., Dick, G., Kačmařík, M., Brožková, R., Zus, F., Brenot, H., ... & Kaplon, J. (2016). Benchmark campaign and case study episode in central Europe for development and assessment of advanced GNSS tropospheric models and products. Atmospheric Measurement Techniques, 9(7), 2989-3008. doi:10.5194/amt-9-2989-2016

Dousa, J., Vaclavovic, P., & Elias, M. (2017). Tropospheric products of the second GOP European GNSS reprocessing (1996–2014). Atmospheric Measurement Techniques, 10(9), 3589-3607. doi:10.5194/amt-10-3589-2017

Gendt, G., Dick, G., Reigber, C., Tomassini, M., Liu, Y., & Ramatschi, M. (2004). Near real time GPS water vapor monitoring for numerical weather prediction in Germany. Journal of the Meteorological Society of Japan. Ser. II, 82(1B), 361-370. doi:10.2151/jmsj.2004.361

Giannaros, C., Kotroni, V., Lagouvardos, K., Giannaros, T. M., & Pikridas, C. (2020). Assessing the impact of GNSS ZTD data assimilation into the WRF modeling system during high-impact rainfall events over Greece. Remote Sensing, 12(3), 383. doi:10.3390/rs12030383

Hersbach, H., Bell, B., Berrisford, P., Hirahara, S., Horányi, A., Muñoz-Sabater, J., ... & Thépaut, J. N. (2020). The ERA5 global reanalysis. Quarterly Journal of the Royal Meteorological Society, 146(730), 1999-2049. doi: 10.1002/qj.3803

Iwabuchi, T., Miyazaki, S. I., Heki, K., Naito, I., & Hatanaka, Y. (2003). An impact of estimating tropospheric delay gradients on tropospheric delay estimations in the summer using the Japanese nationwide GPS array. Journal of Geophysical Research: Atmospheres, 108(D10). doi:10.1029/2002JD002214

Kačmařík, M., Douša, J., Zus, F., Václavovic, P., Balidakis, K., Dick, G., & Wickert, J. (2019, June). Sensitivity of GNSS TGs to processing options. In Annales Geophysicae (Vol. 37, No. 3, pp. 429-446). Copernicus GmbH. doi:https:10.5194/angeo-37-429-2019

Li, X., Dick, G., Lu, C., Ge, M., Nilsson, T., Ning, T., ... & Schuh, H. (2015). Multi-GNSS meteorology: real-time retrieving of atmospheric water vapor from BeiDou, Galileo, GLONASS, and GPS observations. IEEE Transactions on Geoscience and Remote Sensing, 53(12), 6385-6393. doi:10.1109/TGRS.2015.2438395

Lindskog, M., Ridal, M., Thorsteinsson, S., & Ning, T. (2017). Data assimilation of GNSS zenith total delays from a Nordic processing centre. Atmospheric Chemistry and Physics, 17(22), 13983-13998. doi:10.5194/acp-17-13983-2017

Mahfouf, J. F., Ahmed, F., Moll, P., & Teferle, F. N. (2015). Assimilation of zenith total delays in the AROME France convective scale model: a recent assessment. Tellus A: Dynamic Meteorology and Oceanography, 67(1), 26106. doi:10.3402/tellusa.v67.26106

Mascitelli, A., Federico, S., Fortunato, M., Avolio, E., Torcasio, R. C., Realini, E., ... & Dietrich, S. (2019). Data assimilation of GPS-ZTD into the RAMS model through 3D-Var: preliminary results at the regional scale. Measurement Science and Technology, 30(5), 055801. doi:10.1088/1361-6501/ab0b87

Mascitelli, A., Federico, S., Torcasio, R. C., & Dietrich, S. (2021). Assimilation of GPS Zenith Total Delay estimates in RAMS NWP model: Impact studies over central Italy. Advances in Space Research, 68(12), 4783-4793. doi:10.1016/j.asr.2020.08.031

Morel, L., Pottiaux, E., Durand, F., Fund, F., Boniface, K., de Oliveira Junior, P. S., & Van Baelen, J. (2015). Validity and behaviour of TGs estimated by GPS in Corsica. Advances in Space Research, 55(1), 135-149. doi:10.1016/j.asr.2014.10.004

Parrish, D. F., & Derber, J. C. (1991). The National Meteorological Center's spectral statistical interpolation analysis system. url:https://repository.library.noaa.gov/view/noaa/11449

Poli, P., Moll, P., Rabier, F., Desroziers, G., Chapnik, B., Berre, L., ... & El Guelai, F. Z. (2007). Forecast impact studies of zenith total delay data from European near real-time GPS stations in Météo France 4DVAR. Journal of Geophysical Research: Atmospheres, 112(D6). doi:10.1029/2006JD007430

https://doi.org/10.5194/egusphere-2025-19
Preprint. Discussion started: 7 February 2025


Powers, J. G., Klemp, J. B., Skamarock, W. C., Davis, C. A., Dudhia, J., Gill, D. O., ... & Duda, M. G. (2017). The weather research and forecasting model: Overview, system efforts, and future directions. Bulletin of the American Meteorological Society, 98(8), 1717-1737. doi:10.1175/BAMS-D-15-00308.1

Risanto, C. B., Castro, C. L., Arellano, A. F., Moker, J. M., & Adams, D. K. (2021). The impact of assimilating GPS precipitable water vapor in convective-permitting WRF-ARW on North American Monsoon precipitation forecasts over Northwest Mexico. Monthly Weather Review, 149(9), 3013-3035. doi:10.1175/MWR-D-20-0394.1

Rohm, W., Guzikowski, J., Wilgan, K., & Kryza, M. (2019). 4DVAR assimilation of GNSS zenith path delays and precipitable water into a numerical weather prediction model WRF. Atmospheric Measurement Techniques, 12(1), 345-361. doi:10.5194/amt-12-345-2019

Singh, R., Ojha, S. P., Puviarasan, N., & Singh, V. (2019). Impact of GNSS signal delay assimilation on short range weather forecasts over the Indian region. Journal of geophysical research: atmospheres, 124(17-18), 9855-9873. doi:10.1029/2019JD030866

Skamarock, W. C., Klemp, J. B., Dudhia, J., Gill, D. O., Barker, D., Duda, M. G., … Powers, J. G. (2008). A Description of the Advanced Research WRF Version 3 (No. NCAR/TN-475+STR). University Corporation for Atmospheric Research. doi:10.5065/D68S4MVH

Thundathil, R., Zus, F., Dick, G., & Wickert, J. (2024). Assimilation of GNSS TGs into the Weather Research and Forecasting (WRF) model version 4.4. 1. Geoscientific Model Development, 17(9), 3599-3616. doi:10.5194/gmd-17-3599-2024

Václavovic, P., Douša, J., and Györi, G.: G-Nut software library – State of development and first results, Acta Geodyn. Geomater., 10, 431–436, https://doi.org/10.13168/AGG.2013.0042, 2014.

Vedel, H., & Huang, X. Y. (2004). Impact of ground based GPS data on numerical weather prediction. Journal of the Meteorological Society of Japan. Ser. II, 82(1B), 459-472. doi:10.2151/jmsj.2004.459

Walpersdorf, A., Calais, E., Haase, J., Eymard, L., Desbois, M., & Vedel, H. (2001). Atmospheric gradients estimated by GPS compared to a high resolution numerical weather prediction (NWP) model. Physics and Chemistry of the Earth, Part A: Solid Earth and Geodesy, 26(3), 147-152. doi:10.1016/S1464-1895(01)00038-2

Wickert, J., Dick, G., Schmidt, T., Asgarimehr, M., Antonoglou, N., Arras, C., ... & Sem, M. (2020). GNSS remote sensing at GFZ: Overview and recent results. ZfV-Zeitschrift für Geodäsie, Geoinformation und Landmanagement, (zfv 5/2020). doi:10.12902/zfv-0320-2020

Yan, X., Ducrocq, V., Poli, P., Hakam, M., Jaubert, G., & Walpersdorf, A. (2009). Impact of GPS zenith delay assimilation on convective-scale prediction of Mediterranean heavy rainfall. Journal of Geophysical Research: Atmospheres, 114(D3). doi:10.1029/2008JD011036

Yang, S. C., Huang, Z. M., Huang, C. Y., Tsai, C. C., & Yeh, T. K. (2020). A case study on the impact of ensemble data assimilation with GNSS-zenith total delay and radar data on heavy rainfall prediction. Monthly Weather Review, 148(3), 1075-1098. doi:10.1175/MWR-D-18-0418.1

https://doi.org/10.5194/egusphere-2025-19
Preprint. Discussion started: 7 February 2025


Zus, F., Thundathil, R., Dick, G., & Wickert, J. (2023). Fast Observation Operator for Global Navigation Satellite System TGs. Remote Sensing, 15(21), 5114. doi:10.3390/rs15215114

Zus, F.; Douša, J.; Kačmařík, M.; Václavovic, P.; Dick, G.; Wickert, J. Estimating the Impact of Global Navigation Satellite System Horizontal Delay Gradients in Variational Data Assimilation. Remote Sens. 2019, 11, 41. https://doi.org/10.3390/rs11010041

https://doi.org/10.5194/egusphere-2025-19
Preprint. Discussion started: 7 February 2025


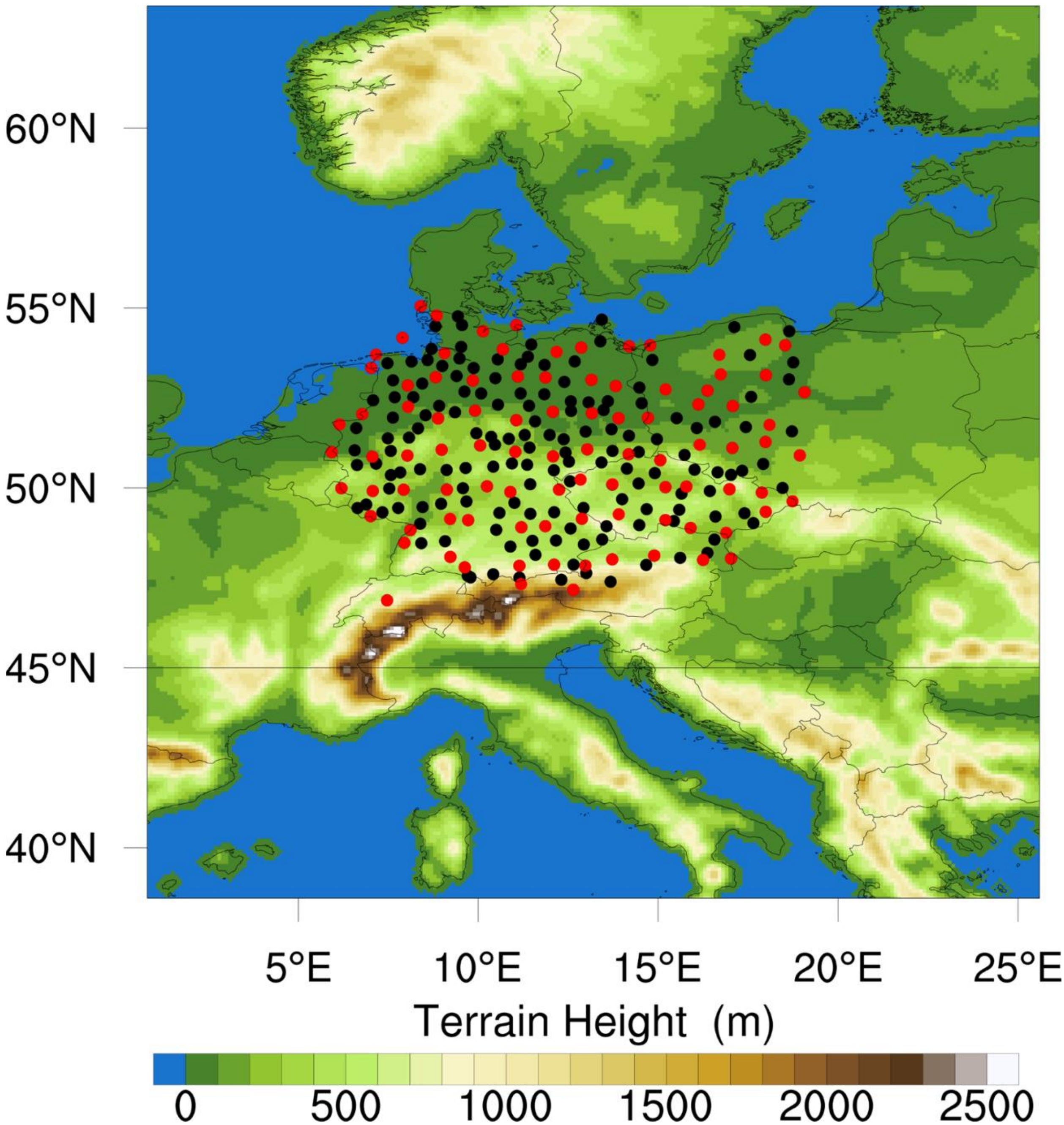


405 **Figure 1.** The WRF model domain with terrain height representation. The GNSS stations in the assimilation study are depicted in red to signify the sparse network with a 1-degree density, while the combination of black and red indicates the dense network with a 0.5-degree density.

https://doi.org/10.5194/egusphere-2025-19
Preprint. Discussion started: 7 February 2025


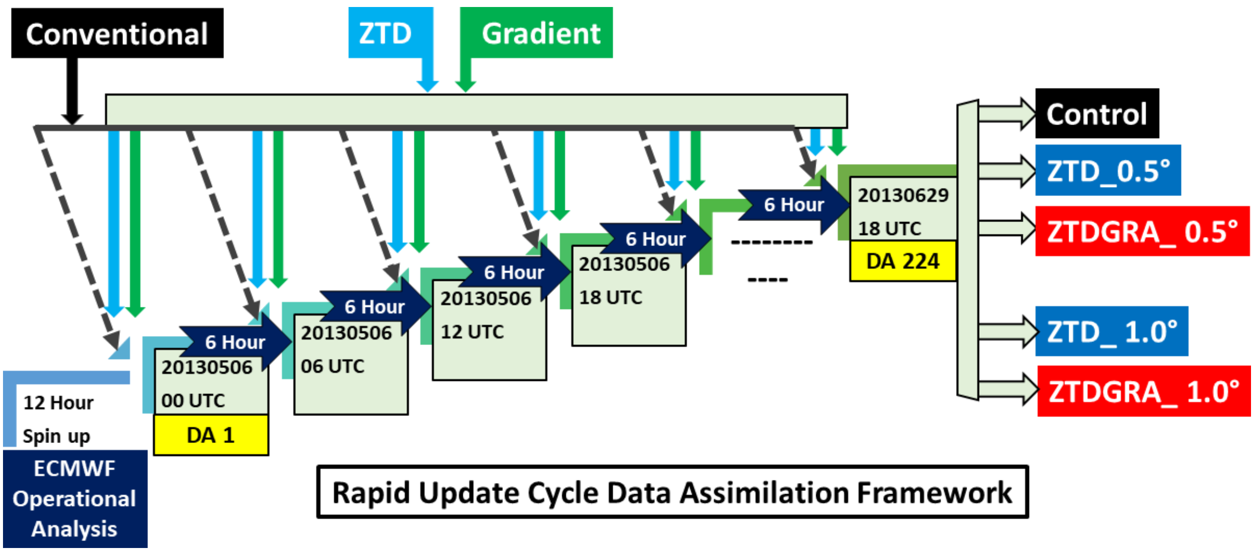


**Figure 2.** Schematic of the 3D-Var rapid update cycle initialized from the ECMWF operational analysis. A spin-up of 12 h was performed until 00:00 UTC on 6 May 2013. Five experiments with different setups are performed in two sets. The first set comprises a control run assimilating conventional data, a ZTD_0.5° run assimilating ZTDs on top of the control run, and a ZTDGRA_0.5° run assimilating ZTD and TGs on top of the control run. These experiments are conducted with the observations from the (dense) 0.5-degree station network. The second set runs are ZTD_1_0° and ZTDGRA_1_0° with the assimilation of observations from the (sparse) 1-degree station network.

https://doi.org/10.5194/egusphere-2025-19
Preprint. Discussion started: 7 February 2025


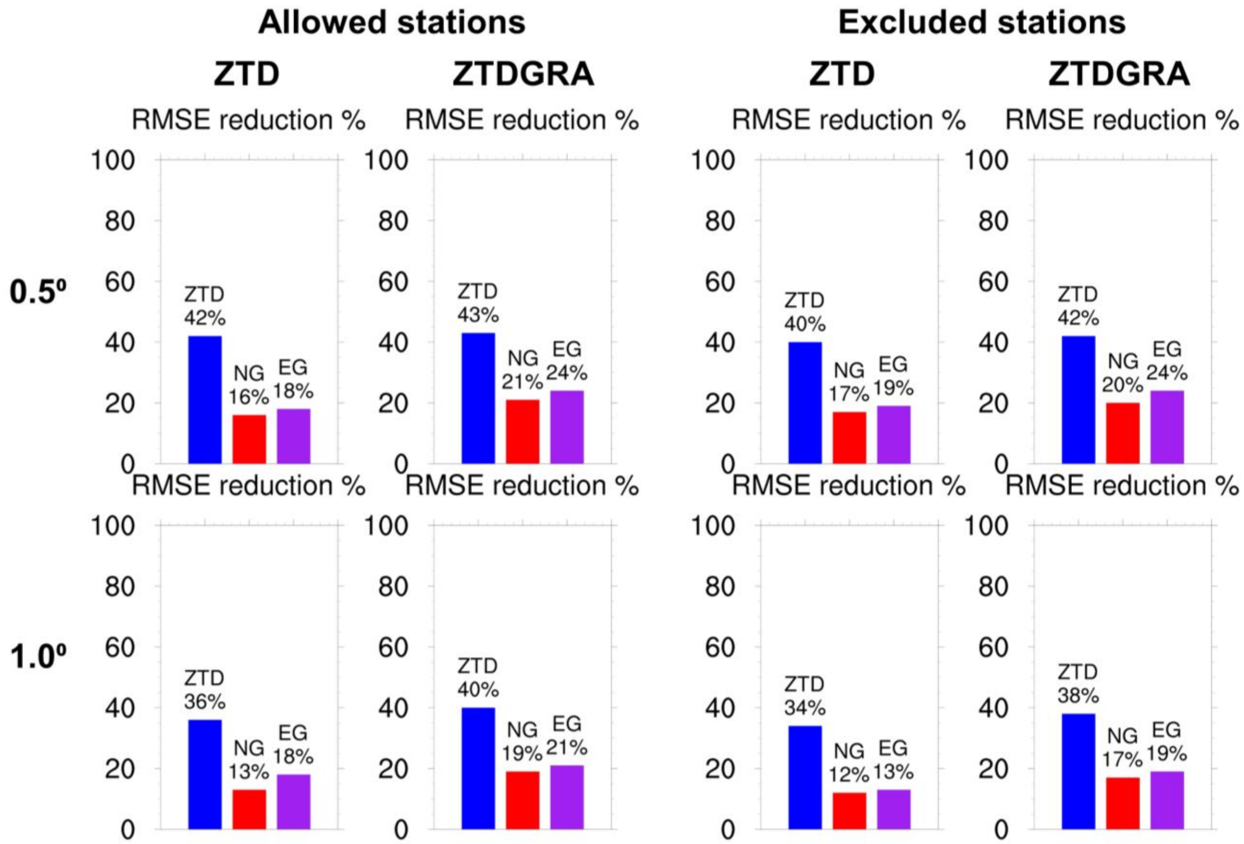


**Figure 3.** RMSE comparison w.r.t stations: assimilated or "allowed" and independent or "excluded." The plot shows the RMSE reduction w.r.t the control run in percentage. Please refer to the appendices for a detailed plot.

https://doi.org/10.5194/egusphere-2025-19
Preprint. Discussion started: 7 February 2025


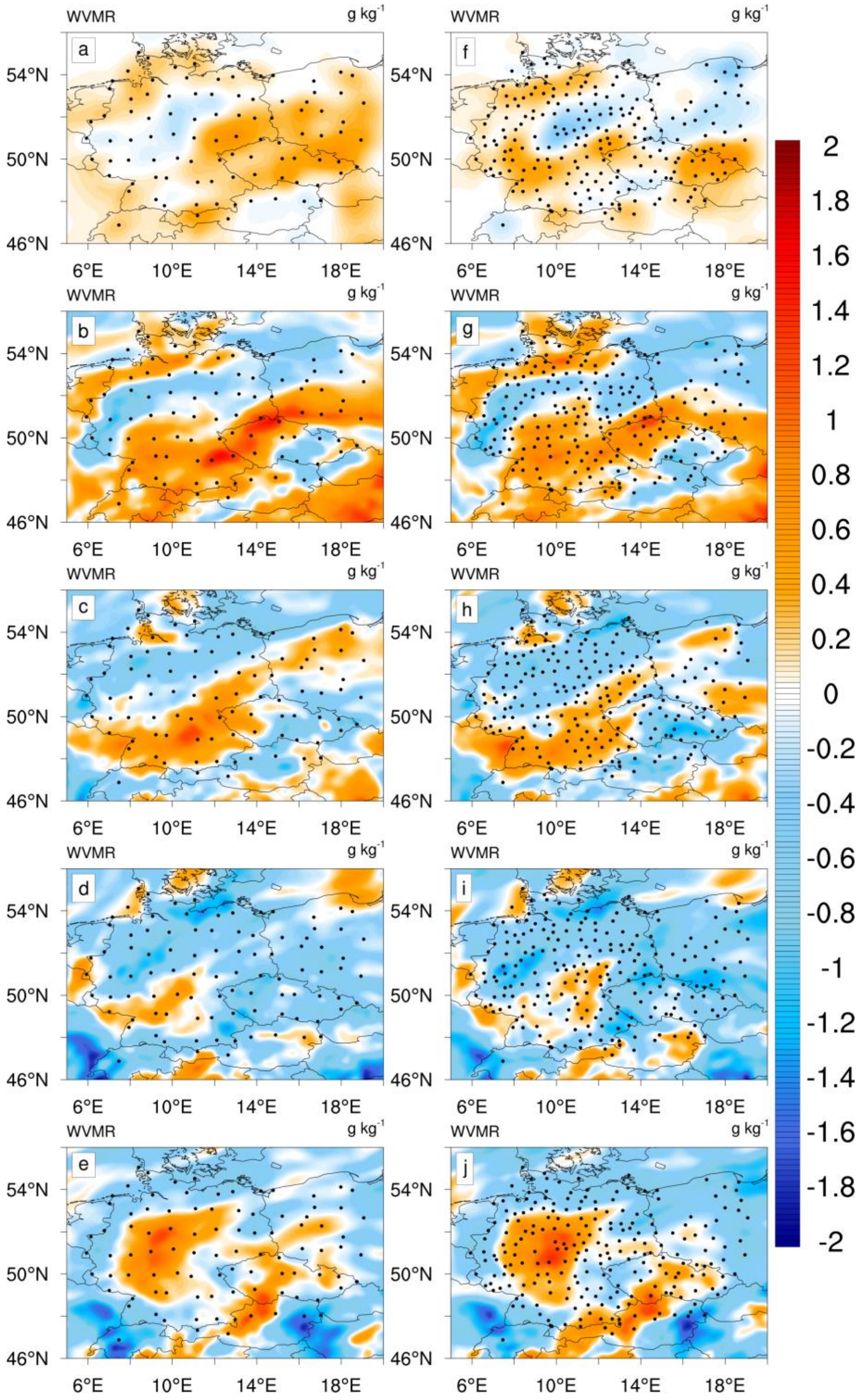

https://doi.org/10.5194/egusphere-2025-19
Preprint. Discussion started: 7 February 2025


**Figure 4.** Spatial comparison of the evolution of the analysis increments of ZTDGRA_1.0° (left column) and ZTD_0.5° (right column) runs for the first five assimilation cycles. The stations used for the respective assimilation runs are depicted by black dots.

https://doi.org/10.5194/egusphere-2025-19
Preprint. Discussion started: 7 February 2025


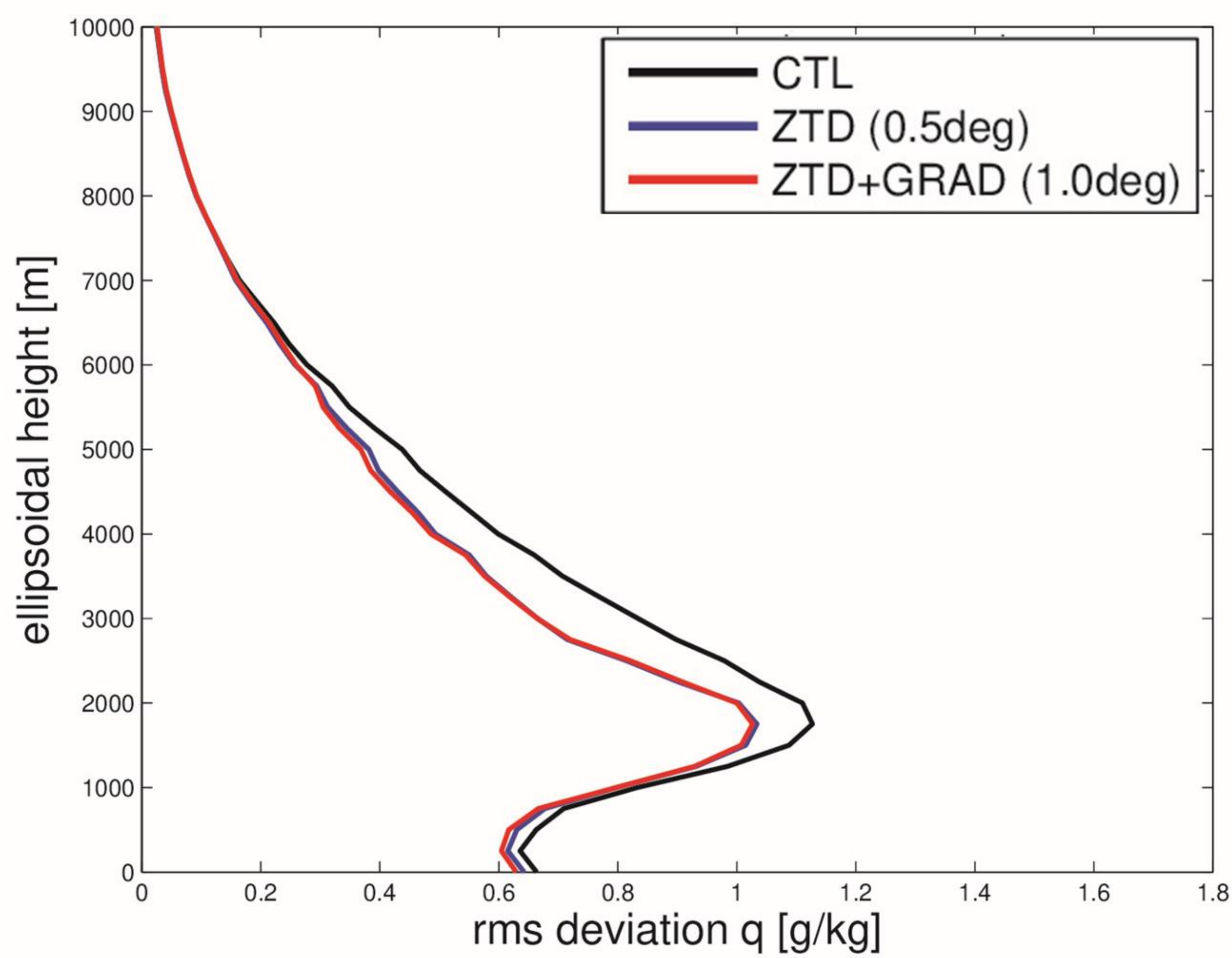


**Figure 5.** The RMSE profile comparison of the ZTD_0.5° and ZTDGRA_1.0° runs. Profiles were compared at five selected stations for 220 DA cycles, totaling 1100 profiles for the average plot.

430

https://doi.org/10.5194/egusphere-2025-19
Preprint. Discussion started: 7 February 2025


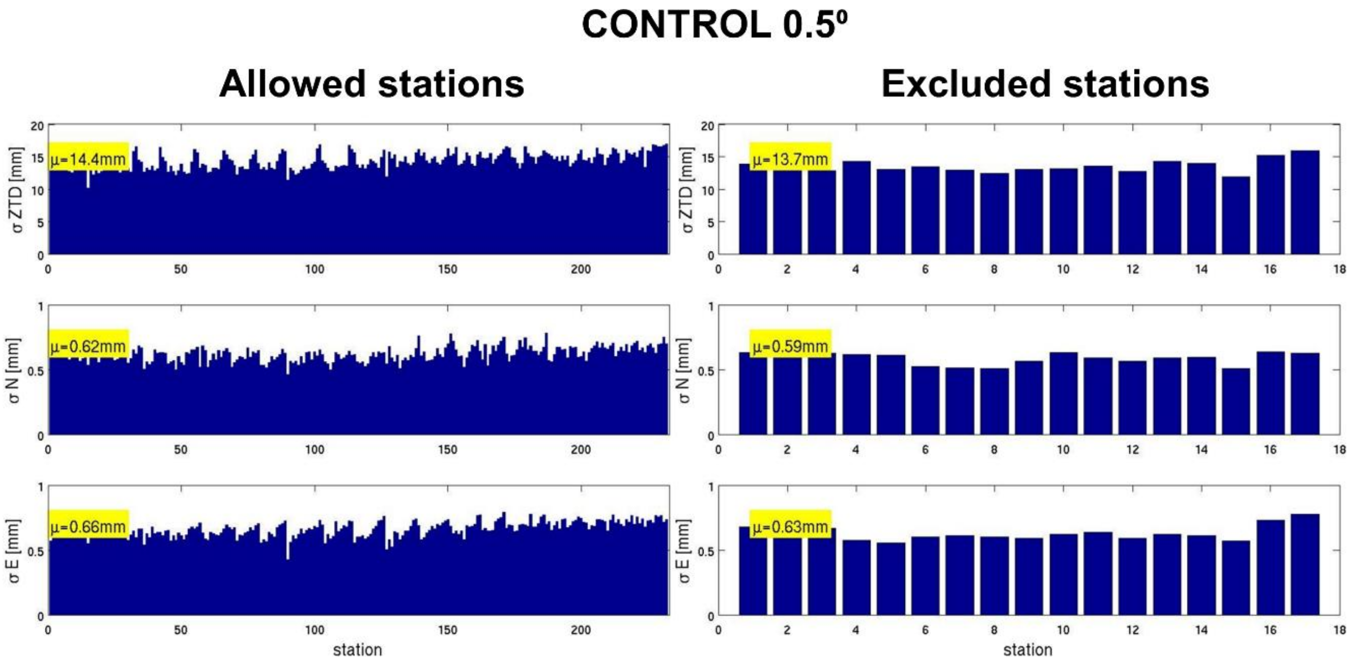


**Figure A1.** Station specific standard deviation of the Control run with dense network configuration. ZTD, North gradient, and East gradient of the allowed and excluded stations are shown on the left column and right column, respectively. The mean values are shown as text with the yellow background.

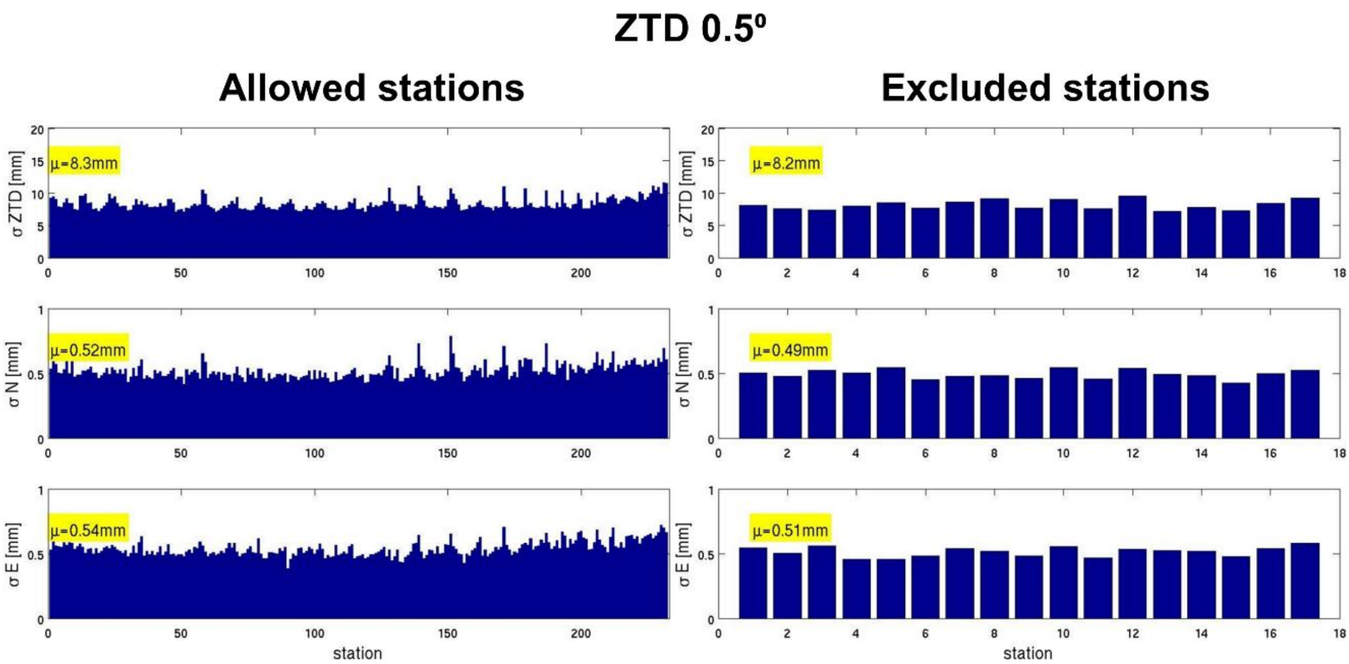


**Figure A2.** Same as Figure A1, but for ZTD run in the dense network configuration.

https://doi.org/10.5194/egusphere-2025-19
Preprint. Discussion started: 7 February 2025


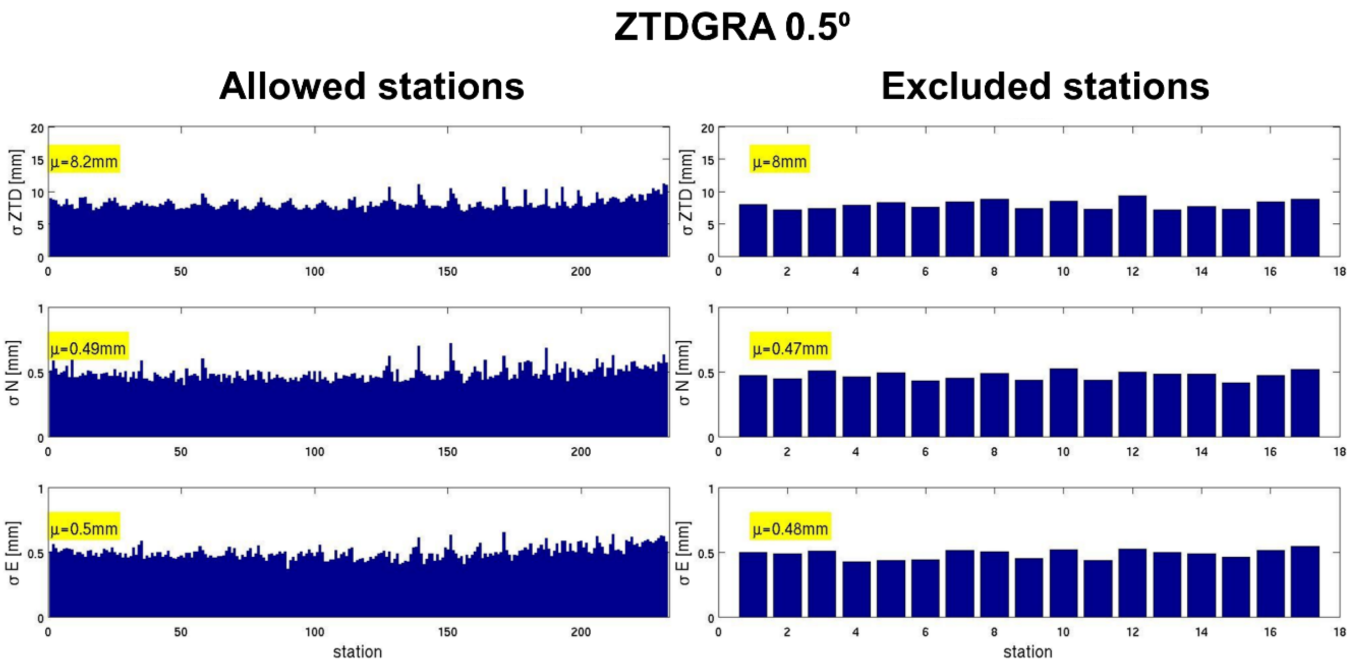


**Figure A3.** Same as Figure A1, but for ZTDGRA run in the dense network configuration.

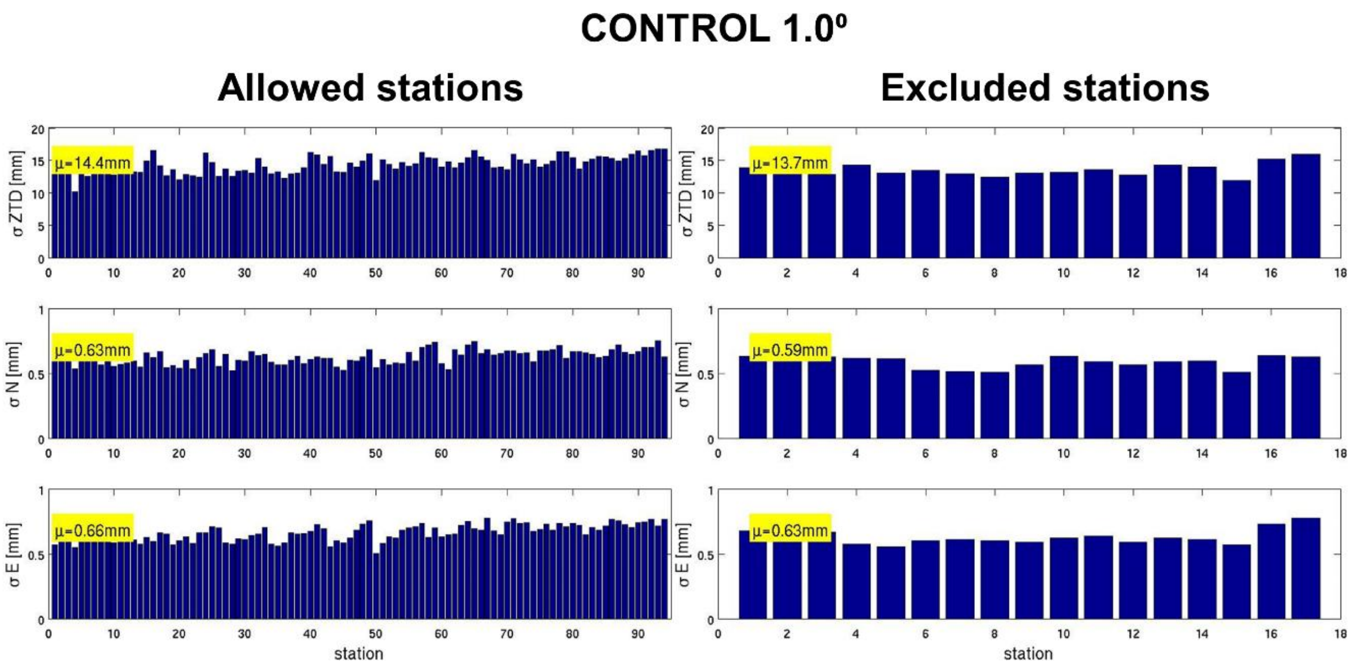


**Figure A4.** Same as Figure A1, but for Control run in the sparse network configuration.

https://doi.org/10.5194/egusphere-2025-19
Preprint. Discussion started: 7 February 2025


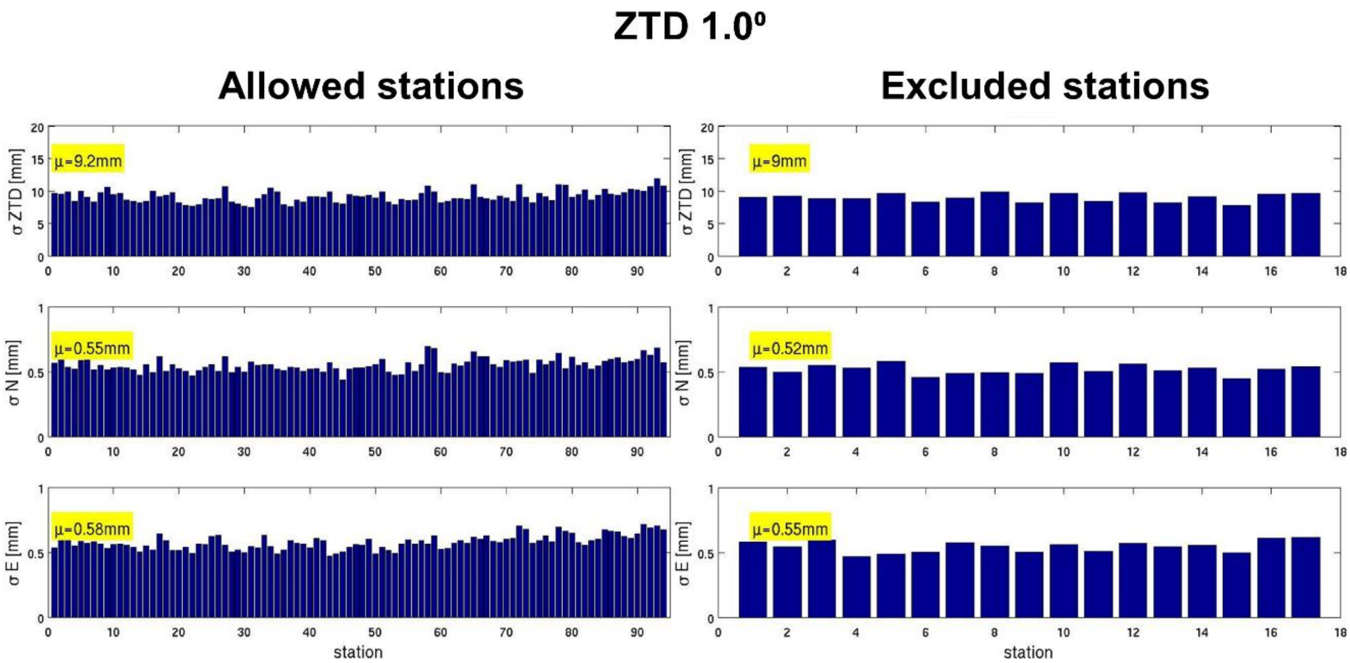

**Figure A5.** Same as Figure A1, but for ZTD run in the sparse network configuration.

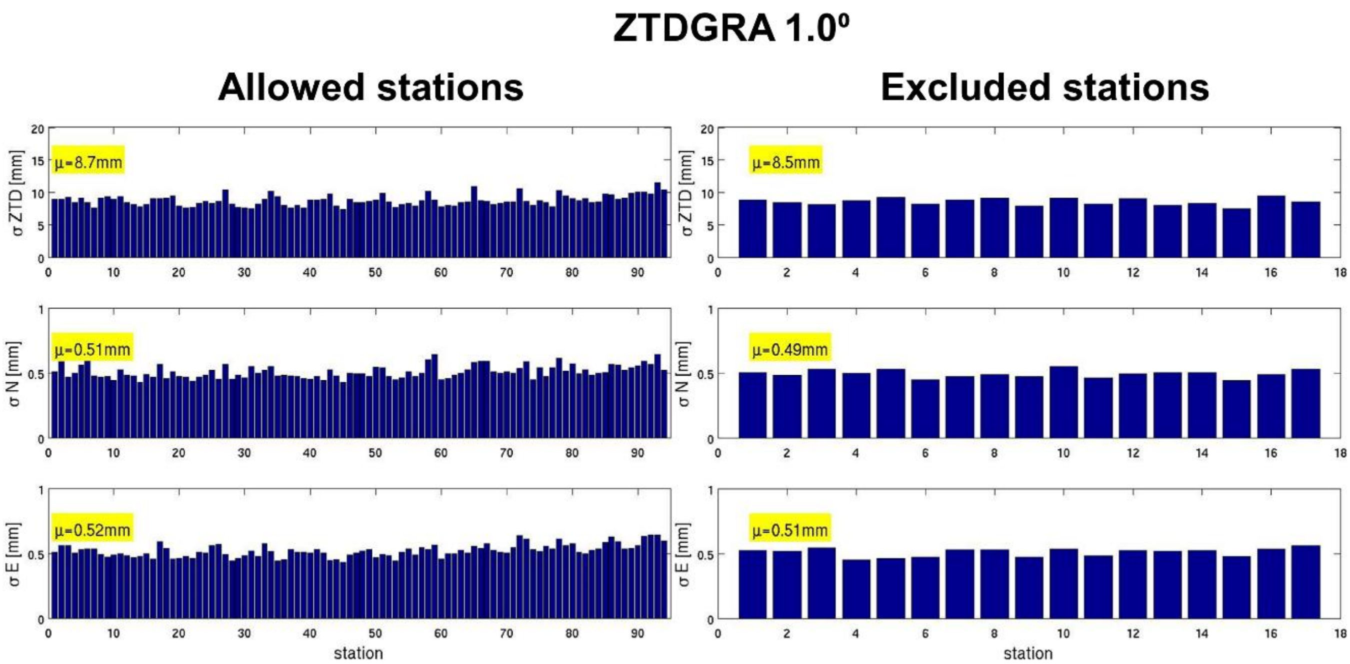

**Figure A6.** Same as Figure A1, but for ZTDGRA run in the sparse network configuration.

https://doi.org/10.5194/egusphere-2025-19
Preprint. Discussion started: 7 February 2025


| **Allowed stations** | | | | | | |
|---|---|---|---|---|---|---|
| **Exp.** | **Standard deviation (0.5°)** | | | **Standard deviation (1.0°)** | | |
| | **ZTD** | **N-Gradient** | **E-Gradient** | **ZTD** | **N-Gradient** | **E-Gradient** |
| **Control run** | 14.4 | 0.62 | 0.66 | 14.4 | 0.63 | 0.66 |
| **ZTD run** | 8.3 | 0.52 | 0.54 | 9.2 | 0.55 | 0.58 |
| **ZTDGRA run** | 8.2 | 0.49 | 0.5 | 8.7 | 0.51 | 0.52 |
| **Excluded stations** | | | | | | |
| **Exp.** | **Standard deviation (0.5°)** | | | **Standard deviation (1.0°)** | | |
| | **ZTD** | **N-Gradient** | **E-Gradient** | **ZTD** | **N-Gradient** | **E-Gradient** |
| **Control run** | 13.7 | 0.59 | 0.63 | 13.7 | 0.59 | 0.63 |
| **ZTD run** | 8.2 | 0.49 | 0.51 | 9 | 0.52 | 0.55 |
| **ZTDGRA run** | 8 | 0.47 | 0.48 | 8.5 | 0.49 | 0.51 |

**Table A1.** Mean standard deviation derived out of station specific standard deviation. The allowed stations and the excluded
450 stations are compared. The grey background signifies that the values are close for ZTD dense network and ZTDGRA sparse network.